Physica B 455 (2014) 35–38

Contents lists available at ScienceDirect

Physica B

journal homepage: www.elsevier.com/locate/physb

The spatial distribution of temperature and oxygen deficiency in spark-plasma sintered superconducting Bi-based materials

E. Govea-Alcaide [a], J.E. Pérez-Fernández [a], I.F. Machado [b], R.F. Jardim [c,*]

[a] Departamento de Ciencias Básicas, Facultad de Ciencias Técnicas, Universidad de Granma, Apdo. 21, P.O. Box 85100, Bayamo, Cuba
[b] Departamento de Engenharia Mecatrônica e Sistemas Mecânicos, Escola Politécnica, Universidade de São Paulo, 05508-900 São Paulo, SP, Brazil
[c] Instituto de Física, Universidade de São Paulo, CP 66318, 05315-970 São Paulo, SP, Brazil

ARTICLE INFO

Article history:
Received 21 December 2013
Accepted 18 July 2014
Available online 7 August 2014

Keywords:
Bi-based superconductor
Granular material
Spark-plasma sintering
Finite element method
Transport properties

ABSTRACT

Pre-reacted powders of $(Bi–Pb)_2Sr_2Ca_2Cu_3O_{10+\delta}$ (Bi-2223) were consolidated by using the spark plasma sintering (SPS) technique under vacuum and at different consolidate temperatures T_D. X-ray diffraction patterns revealed that the dominant phase in all SPS samples is the Bi-2223 phase, but traces of the $Bi_2Sr_2CaCu_2O_{10+x}$ (Bi-2212) phase were identified. We have found that the transport properties of SPS samples depend on their oxygen content because the SPS process is performed under vacuum. Simulations by using the finite element method (FEM) were performed for determining the actual temperature in which powders are consolidated. From these results we have inferred that SPS samples are oxygen deficient and such a deficiency is more marked near the grain boundaries, suggesting the occurrence of grains with core–shell morphology. We also argued that the width of the shell depends on the consolidation temperature, a feature corroborated by the FEM simulations.

© 2014 Elsevier B.V. All rights reserved.

The spark plasma sintering (SPS) is an effective, unconventional method for promoting densification of powders by the simultaneous action of a high direct electric current through graphite dies and uniaxial pressure [1]. In high-T_c cuprate superconductors, the use of SPS may be a difficult task because the process occurs under vacuum, and the general physics properties of these materials are very sensitive to the oxygen content. Such an oxygen-dependent features are much less pronounced in materials belonging to the Bi–Sr–Ca–Cu–O (BSCCO) system [2], making the application of the SPS method useful for promoting densification of these families of high-T_c cuprates superconductors. However, up to now there are few studies regarding the use of SPS in the BSCCO system. In the last decade, a study of the influence of the SPS conditions on the formation of $(Bi,Pb)_2Sr_2CaCu_2O_{8+\delta}$ (Bi-2212) and $(Bi,Pb)_2Sr_2Ca_2Cu_3O_{10+\delta}$ (Bi-2223) phases was conducted [3]. The authors obtained SPS samples under different consolidation temperatures T_D and times and the net result was the production of samples composed of extra phases, as inferred from X-ray diffraction analysis. Moreover, a recent study on SPS Bi-2223 samples suggested that T_D not only has a strong influence on the phase composition but also in the oxygen content of the Bi-2223 ceramics [4]. These results indicated that one of the most important challenges of any SPS process, even performed under vacuum, is to determine precisely the consolidation temperature in which the powder is subjected during the brief time interval of the SPS process.

Within this scenario, the main motivation of this work is to disclose the intricate balance between T_D, phase composition, and the oxygen content of samples prepared by the SPS method. For this purpose, we have consolidated pre-reacted powders of the $Bi_{1.65}Pb_{0.35}Sr_2Ca_2\ Cu_3O_{10+\delta}$ compound by spark-plasma sintering. The finite element method (FEM) was used for optimizing the consolidation temperature in order to produce single phase materials. The SPS samples were characterized by X-ray diffraction (XRD), scanning electron microscopy (SEM), temperature dependence of the electrical resistivity, and voltage–current characteristics.

The schematic drawing of the consolidation system is displayed in Fig. 1(a). It is composed of two inconel electrodes, six graphite spacers, the die with two plungers, and the sample, the latter located in the center of the apparatus. For each of the above domains, the electro-thermal process is described by a two coupled partial differential equations: one related to the charge conservation law and the other one associated with the heat transfer process [6,7]:

$$\nabla \cdot J = 0, \tag{1}$$

$$\rho c_p(T)\frac{\partial T}{\partial t} - \nabla \cdot (k\nabla T) = q_i. \tag{2}$$

Here, T is the temperature, ρ is the density, $q_i = JE$ is the heat loss by Joule effect, $J = E/\rho_e(T)$ is the electric current density, $\rho_e(T)$ is

* Corresponding author.
E-mail address: rjardim@if.usp.br (R.F. Jardim).

http://dx.doi.org/10.1016/j.physb.2014.07.040
0921-4526/© 2014 Elsevier B.V. All rights reserved.

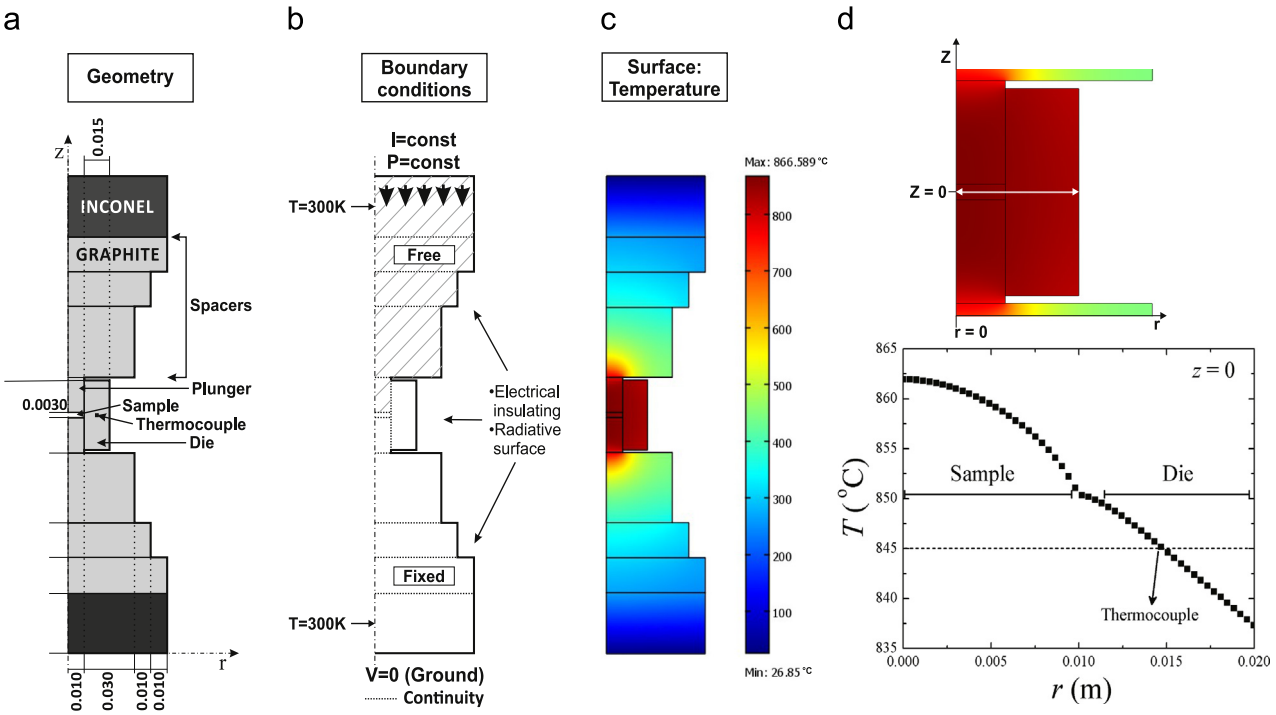

Fig. 1. (a) Schematic drawing of the consolidation system, (b) boundary conditions, (c) simulation by FEM of the temperature distribution of the whole system (see details in the text), and (d) expanded view of the temperature distribution of the die-sample region and the radial temperature profile for $z=0$.

the temperature dependence of the electrical resistivity, $c_p(T)$ is the heat capacity as a function of temperature, and $k(T)$ is the thermal conductivity. Values for each parameter are assigned for each material or domain in the geometry, i.e., the inconel, the graphite, and the Bi-2223 sample. Table 1 displays the parameters used in the FEM simulations for the Bi-2223 sample [4,9]. The parameters used for both the graphite and the inconel 600 are reported elsewhere [6,8]. The initial and boundary conditions used for solving Eqs. (1) and (2) are displayed in Fig. 1(b). The initial temperature was set to be 300 K and the heat losses by conduction and/or convection through the gas were neglected because the process occurs in vacuum. All the free surfaces exposed to the vacuum chamber have heat losses by radiation, given by $\dot{q}_{rad}=\sigma_s\varepsilon(T_d^4-T_0^4)$, where T_d is the temperature of the free surfaces, σ_s is Stefan–Boltzmann's constant, $\varepsilon=0.3$ (0.69) is the graphite (inconel 600) emissivity, and $T_0=300$ K is the temperature of the wall of the chamber. The temperature of both the upper and lower inconel electrodes was 300 K and the electrical current density is injected from the top to the bottom. Finally, the electrothermal equations (1) and (2) were solved by the FEM by using the COMSOL Multiphysics™ package.

Powders of $Bi_{1.65}Pb_{0.35}Sr_2Ca_2Cu_3O_{10+\delta}$ (Bi-2223) were prepared by the traditional solid state reaction method, as described elsewhere [4]. The final consolidation of the samples was performed in a SPS 1050 Dr Sinter® apparatus. Powders of Bi-2223 were placed inside a cylindrical graphite die, between two graphite plungers, as displayed in Fig. 1(a). The die was then placed inside the chamber of the SPS apparatus and sintering was performed under vacuum (roughly from 10 to ~30 Pa) and an uniaxial pressure along the z-axis of 50 MPa. In order to study the influence of the consolidation temperature, T_D, the samples were subjected to different temperatures $T_D=750$, 830, and 845 °C. The above samples were labeled as **S75**, **S83**, and **S85**. The heating rate was HR = 145, 160, and 163 °C/min, and the dwell time was 5 min for all samples. Further details of the consolidation process employed for producing the samples are described elsewhere [4]. Additionally, for comparison reasons, ~4 g of the starting powder was *cold pressed* inside the SPS apparatus and the resulting pellet was sintered at 845 °C in air for 2400 min. This sample (**R84**) will thereafter be referred as a *reference sample*. Finally, the density, ρ, of all pellets was determined by the Archimedes method.

Table 1
Parameters of the Bi-2223 phase used in the FEM simulations [4,9]: ρ is its density, $\rho_e(T)$ is the electrical resistivity as a function of temperature, $c_p(T)$ is the heat capacity as a function of temperature, and $k(T)$ is the thermal conductivity.

Properties	Value	Units
ρ	5700	kg/m^3
$\rho_e(T)$	$0.8\times10^{-6}+0.8\times10^{-8}T$	Ωm
$c_p(T)$	$131.6+0.77\,T$	J/kg K
$k(T)$	$0.27+1.95\times10^{-3}T$	W/m K

The phase identification was evaluated, in both powder and bulk samples, by means of X-ray diffraction patterns obtained in a Bruker-AXS D8 Advance diffractometer. These measurements were performed at room temperature using Cu Kα radiation in the $3\le 2\theta\le 80^\circ$ range with a 0.05° (2θ) step size, and 5 s counting time.

The temperature dependence of the electrical resistivity, $\rho(T)$, and the current–voltage characteristics $I\times V$ measurements were performed in a closed cycle cryogenics refrigerator ARS-4HW/DE-202N attached to a temperature controller Lakeshore model 331S. Typical dimensions of the samples were $t=0.5$ mm (thickness), $w=2$ mm (width), and $l=10$ mm (length). More details of these measurements are given elsewhere [4].

The optimum sintering temperature for producing single-phase Bi-2223 is $T_s\sim845$ °C [5]. In addition to this, samples sintered at temperatures below 845 °C usually exhibit extra phases, as Ca_2PbO_4, Bi-2201, and Bi-2212, and those sintered above T_s, due to the presence of liquid phase, are composed of at least two main phases: Bi-2223 and Bi-2212 [5]. Motivated by these experimental results, the conducted simulations of the SPS process were performed by assuming $T\sim845$ °C in the position of the thermocouple, i.e., at $z=0$ and $r=0.015$ m (see Fig. 1(a)). Under these

conditions, the calculated surface plot of the spatial temperature distribution in the whole SPS system is displayed in Fig. 1(c). As expected, higher temperatures are spatially located close to the die-sample region. Fig. 1(d) also displays an expanded view of this region and the temperature profile along the radial direction and for $z=0$. The results also indicate that the average temperature decreases from $T\sim 862$ °C, in the center of the sample, to $T\sim 837$ °C at the outer surface of the die. The temperature difference between the thermocouple and the center of the sample, estimated from our simulations, is then $\Delta T\sim 17$ °C. Such a result strongly indicates that in the actual SPS process the consolidation temperature T_D may be corrected by subtraction of ~ 15 °C for reaching the optimum sintering temperature of the Bi-2223 phase.

In order to verify the results of the FEM simulations, a sample was consolidated by SPS at $T_D=845$ °C and we emphasize that such a value of T_D refers to the temperature measured by the thermocouple. X-ray powder diffraction patterns of the *reference sample* **R84** and the SPS sample **S85** consolidated at $T_D=845$ °C are displayed in Fig. 2(a) and (b), respectively. The analysis of the pattern of the *reference sample* reveals that all indexed reflections are related to the high-T_c Bi-2223 phase (H(hkl)). However, in the sample **S85** the most intense peaks are related to the low-T_c phase Bi-2212 (L(hkl)). According to the resulting temperature profile of our simulations (see Fig. 1(d)), the actual sintering temperature of the **S85** sample was in the range comprehended between ~ 850 and 860 °C. The X-ray powder diffraction data confirm that, as anticipated by FEM simulations, single-phase Bi-2223 materials are obtained by reducing the consolidation temperature. Motivated by these experimental results and the FEM simulations, we further consolidated other two Bi-2223 samples at lower temperatures: $T_D=750$ and 830 °C. Assuming $\Delta T\approx 15$ °C, the actual temperature in the center of the samples is expected to be ~ 765 and 845 °C. Thereafter, these two Bi-2223 samples will be used to investigate the influence of T_D on their general physical and superconducting properties.

Fig. 2(c) and (d) displays the X-ray powder diffraction patterns of samples **S83** and **S75**, which were SPS at 830 and 750 °C, respectively. The results indicate that in both samples all peaks of the high-T_c Bi-2223 phase are indexed but we have also observed traces of the extra phase Bi-2212, identified by the occurrence of the reflection L(117) (see Fig. 2(c)). The volume fraction of this extra phase was found to remain essentially constant in the two consolidated samples, as displayed in Fig. 2(c) and (d). We mention here that the absence of peaks belonging to other extra phases as Ca_2PbO_4 and Bi-2201 point out for different phase equilibria when the Bi-2223 powders are subjected to high temperatures, under vacuum, and under an uniaxial pressure of 50 MPa.

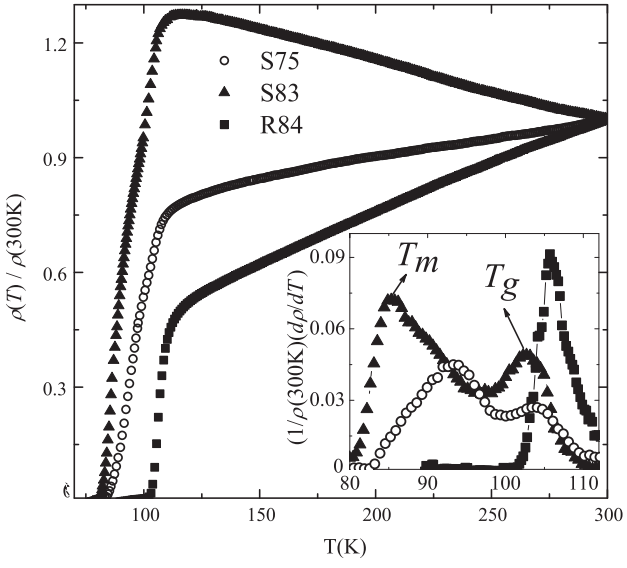

Fig. 2. X-ray diffraction patterns of the powders of samples **R84** (a), **S85** (b), **S75** (c), and **S83** (d). The reflections belonging to the Bi-2223 (H(hkl)) and Bi-2212 (L(hkl)) phases are marked by Miller indexes in (a) and (b), respectively.

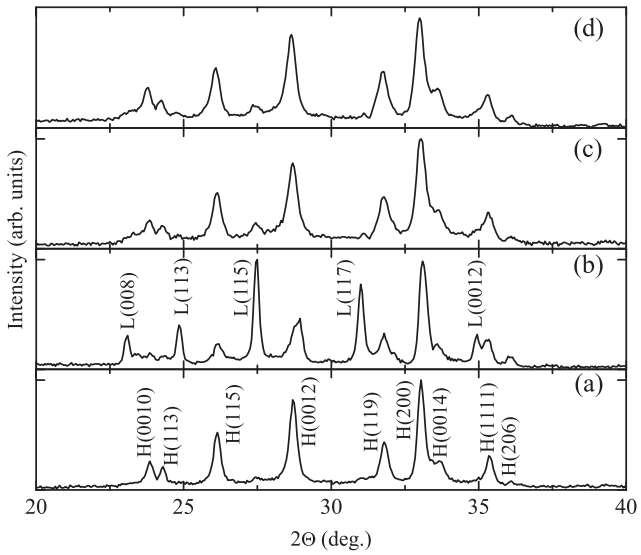

Fig. 3. Normalized $\rho(T)/\rho(300\,K)$ data of samples **S75**, **S83**, and **R84**. The inset displays an expanded view of the first derivative of $\rho(T)$ between 80 and 110 K. In the inset, T_g and T_m are the intra- and the intergranular transition temperatures, respectively.

Fig. 3 displays the normalized temperature dependence of $\rho(T)/\rho(300\text{ K})$ for samples **S83**, **S75**, and the *reference sample* **R84**. The overall behavior of the curves indicate that decreasing the consolidation temperature changes both the normal and superconducting transport properties of the samples. Values of $\rho(T)$ at $T=300$ K decrease from ~ 33 mΩ cm, in sample **S83**, to ~ 10 mΩ cm in **S75**. The data also show that sample **S83** exhibits a semiconductor-like behavior with $\rho(T)$ increasing with decreasing temperature, reaching a maximum in $\rho(T)$, followed by a very broad superconducting transition. The $\rho(T)$ behavior of sample **75PA** displays a typical metallic behavior as also seen in the *reference sample* **84PA**. Along with the electrical resistivity results, the inset of Fig. 3 displays the first derivative of the $\rho(T)/\rho(300\text{ K})$ data in the vicinity of the superconducting transition temperature. We first mention here that the general behavior of the curves is different and the occurrence of the double resistive superconducting transition or the two well-defined peaks in $d\rho(T)/dT$ is only clearly observed in the two SPS samples. These two peaks in $d\rho(T)/dT$ are frequently observed in granular superconductors and are related to the intra- (T_g) and intergranular (T_m) superconducting temperature transitions [11]. Our data indicate that T_g decreases from ~ 105 K to 102 K with increasing consolidation temperature T_D in SPS samples, a similar behavior observed in T_m that assumes values of $T_m\sim 83$ K in **S83** and ~ 94 K in **S75**. On the other hand, the obtained result for the reference sample is quite different since the double resistive superconducting transition is hardly seen, or more appropriately, $T_g=109$ K and $T_m=105$ K.

Such a difference in the transport behavior between SPS samples cannot be only attributed to the presence of extra phases. The phase composition of the two SPS samples **S83** and **S75** is similar, as inferred from X-ray powder diffraction data displayed in Fig. 2. On the other hand, let us take into account that the SPS

process is conducted under vacuum, at high temperatures, and in brief time intervals. Under these circumstances, the results strongly suggest that changes in the $\rho(T)$ behavior of SPS samples may be related to differences in their oxygen content. If this were the case, it would mean that an oxygen deficiency enhancement may occur during the SPS process provided that it occurs in vacuum. In addition to this, the $\rho(T)$ data indicate that the higher the consolidation temperature T_D is, the higher is the oxygen depletion of the samples. As far as T_m is concerned, the results indicate that the expected deoxygenation process preferably takes place near the grain-boundaries, as reported elsewhere [12]. This would affect the transport critical current density $J_c(0)$ measured at 77 K, which was found to be only ~ 2 A/cm^2 in the sample **S83** and ~ 10 A/cm^2 in **S75**. These are small values of $J_c(0)$, compared with ~ 22 A/cm^2 for the *reference sample* **S84**, taking place during the SPS process. The combined results point out to the occurrence of grains with core–shell morphology in SPS samples, where the shell is oxygen deficient and that such a deficiency (width of shell) increases with increasing T_D.

Acknowledgments

The authors acknowledge financial support from the Brazil's agencies CAPES (Grant nos. 104/2010 and 157/2012), FAPESP (Grant no. 2013/07296-2), and CNPq (Grant no. 304112/2010-0), and Petrobras Company.

References

[1] R. Orrù, R. Licheri, A.M. Locci, A. Cincotti, G. Cao, Mater. Sci. Eng. B 63 (2009) 127.
[2] T. Fujii, T. Watanabe, A. Matsuda, Physica C 357 (2001) 173.
[3] P. Badica, G. Aldica, J.R. Groza, M.-C. Bunescu, S. Mandache, Supercond. Sci. Technol. 15 (2002) 32.
[4] E. Govea-Alcaide, I.F. Machado, M. Bertolete-Carneiro, P. Muné, R.F. Jardim, J. Appl. Phys. 112 (2012) 113906.
[5] E. Govea-Alcaide, P. Muné, R.F. Jardim, Physica C 384 (2003) 491.
[6] U. Anselmi-Tamburini, S. Gennari, J.E. Garay, Z.A. Munir, Mater. Sci. Eng. A 394 (2005) 139.
[7] C. Wang, L. Cheng, Z. Zhao, Comput. Mater. Sci. 49 (2010) 351.
[8] G. Molénat, L. Durand, J. Galy, A. Couret, J. Metal. 2010 (2010) 145431.
[9] J.E. Gordon, S. Prigge, S.J. Collocott, R. Driver, Physica C 185 (1991) 1351; T.K. Dey, H.K. Barik, Solid State Commun. 82 (1992) 673; A. Nyilas, K. Osamura, M. Sugano, Supercond. Sci. Technol. 16 (2003) 1036; I. García-Fornaris, A.A. Planas, P. Muné, R.F. Jardim, E. Govea-Alcaide, J. Supercond. Nov. Magn. 23 (2010) 1511.
[11] R.F. Jardim, E.A. Early, M.B. Maple, J. Alloys Compd. 221 (1995) 1.
[12] E. Ozdas, T. Firat, Phys. Rev. B 48 (1993) 9754.